Nucleation and solidification of thin walled ductile iron - Experiments and numerical simulation

Pedersen, Karl Martin; Tiedje, Niels Skat

Published in:
Materials Science and Engineering A: Structural Materials: Properties, Microstructures and Processing

Link to article, DOI:
10.1016/j.msea.2005.08.158

Publication date:
2005

Nucleation and solidification of thin walled ductile iron – Experiments and numerical simulation

Karl Martin Pedersen, and Niels Tiedje

Department of Manufacturing Engineering and Management

Building 425, Technical University of Denmark

DK-2800 Kgs. Lyngby

Denmark

Phone: +45 4525 4720

Fax: +45 4593 4570

E-mail: kmp@ipl.dtu.dk

WWW: http://www.ipl.dtu.dk

Post-print (final draft post-refereering) of article published in:
Materials Science and Engineering A 413-414 (2005) 358-362
Journal homepage: http://www.elsevier.com/wps/product/cws_home/504098
Hyperlink to article: http://www.sciencedirect.com/science/journal/09215093

Abstract

Investigation of solidification of thin walled ductile cast iron has been performed based on experiments and numerical simulation. The experiments were based on temperature measurement and microstructure examination. Both hyper- and near-eutectic alloys have been investigated with plate thicknesses of 2.8, 4.3 and 8 mm.

Temperature measurement revealed that eutectic solidification in the thinner plates (≤4.3mm) was divided into two stages. The first stage was relatively short with little or no recalescence. The second stage was the main stage with a larger recalescence. In 8 mm plates the eutectic solidification had only one main stage. Color etching revealed the presence of austenite dendrites.

Results of the experiments have been compared with a 1-D numerical solidification model that takes into account the precipitation of off-eutectic austenite during the eutectic stage. Simulations reveal that the first stage of eutectic solidification in the thin plates can be explained by growth of off-eutectic austenite.

Keywords

Ductile iron, Solidification, Thin walled casting, Numerical simulation

1. Introduction

In order to save weight e.g. in cars there is an increased interest in casting of thin wall ductile iron. Ductile iron is a Fe-Si-C alloy where C precipitates as graphite spheres, also called nodules. The solidification of ductile iron is complicated, involving nucleation and growth of two different phases. The growth of graphite nodules is thought to be governed by diffusion of C through an austenite shell. Numerical simulation of solidification of ductile iron is therefore normally based on a model where the graphite nodules and austenite shells are growing as two concentric spheres. However experiments have shown that austenite dendrites play an important role in the solidification of ductile iron, even in hypereutectic iron [1-4]. Lesoult et al. have developed a model, which takes into account the presence of off-eutectic austenite or austenite dendrites during solidification [5]. The aim of this paper is to couple experimental results with numerical simulation.

2. Experiment

2.1 Procedure

Four different castings were produced from near eutectic and hypereutectic melts. Ductile cast iron was produced in batches of 90 kg. The chemical analyses of the castings are shown in Table 1. The melt was superheated to 1520°C before being poured into a preheated ladle for magnesium treatment with a Fe-Si-Mg alloy using a tundish sandwich method. The melt for each mould was then poured into a small insulated fiber cup where it was inoculated with 0,1-0,2% Fe-Si alloy before it was poured into the mould. The temperature was measured in the fiber cup with an S-type thermocouple. The moulds were made of chemically bonded sand (Resol-CO_2). The casting layout shown in Fig. 1 had plates with thicknesses of 8, 4.3 and 2.8 mm and a feeder with a thickness of 16 mm. The temperature was measured in the middle of each plate using K-type thermocouples with a 0,2 mm wire. The sample rate for temperature measurement was 500 Hz and every 100 values were averaged to reduce noise giving a time increment of 0.2 second.

Characterization of graphite morphology and matrix microstructure was performed on cross sections of the plates close to the thermocouples. Graphite morphology was characterized using image analysis. The two dimensional spatial size distribution of nodules was converted to a three dimensional size distribution by Schwarts-Saltykov analysis [6]. Nodules below 5 μm were neglected in the counts. The samples were etched in a 3% nital solution to reveal ferrite, pearlite and carbides.

To reveal segregation of Si a color etching, Klemm I [7], was used on casting E. The etching time was about 2 minutes. Low silicon zones will have a blue color while high silicon zones will have a pale color.

2.2 Results

Cooling curves: Examples of measured cooling curves and corresponding dT/dt curves are shown in Fig 2 – 5, and the measured temperatures are shown in Table 2. In all castings there were recalescence, $\Delta T_{rec} = T_{max} - T_{min}$, during the solidification. Concerning ΔT_{rec} there is a major difference between the hypereutectic and eutectic melts. ΔT_{rec} is less than 5°C for the hypereutectic melt (melt E and H) while it is larger for the eutectic melts, about 15-20°C. The plate thickness has only a minor influence on ΔT_{rec}. However looking at the dT/dt curve there is a major difference between the thicker and thinner plates. The thin plates (2.8 and 4.3mm) have a local maximum, T_{12}, on the dT/dt before the T_{min} temperature. This effect is more pronounced in the hypereutectic than in the eutectic melt. For some of the hypereutectic 4.3 mm plates there was even a small recalescence at that place, so there actually were two nucleation events that caused recalescences in these plates. This T_{12} was not present on the cooling curves for any of the 8 mm plates.

Microstructure: The number of nodules pr volume, N, are presented in Table 2. The nodule count is very similar for the eutectic and hypereutectic melts. There is however a difference in the size distribution of the nodules, see Fig. 6. The hypereutectic melts have a bimodal size distribution where most of the nodules are distributed similar to those in the eutectic alloy, combined with a small fraction of large nodules. This effect is only clear in the thinner plates and not in the 8 mm plates. The presence of a group of larger nodules in the hypereutectic melts indicates that they there have nucleated before the eutectic part of the solidification and by that had longer time to grow. The main part of the nodules have nucleated during the eutectic part of the solidification.

In some of the 4.3 mm plates there were a few centerline carbides, probably because of segregation of Si during solidification. The 2.8 mm plate in casting F had some carbides, otherwise the castings solidified without carbides.

The color etching on casting E revealed dendrites with length up to 1 mm in the 4.3 and 2.8 mm plates. In the 8mm plate only few shorter dendrites have been observed. The presence of dendrites seems to be more pronounced in the thinner plates than in the thicker plates.

3. Numerical modeling

The 1-D numerical simulation is based on the solidification model presented by Lesoult, Castro and Lacaze [5, 8]. The model assumes that during the eutectic

solidification the solidification path in the phase diagram will follow the extrapolation of the austenite liquidus. If the growth rate of the austenite shell around the graphite nodules is to low compared to equilibrium in the phase diagram the remaining austenite will precipitates as off-eutectic austenite. Nucleation of graphite nodules is based on a modified Oldfield model:

$$dN = A_n \left(\Delta T_L^g\right)^{n-1} f_L \frac{d\left(\Delta T_L^g\right)}{dt} dt$$

$$\text{when} \quad \frac{d\left(\Delta T_L^g\right)}{dt} > 0$$

$$dN = 0 \quad \text{when} \quad \frac{d\left(\Delta T_L^g\right)}{dt} < 0$$

where N is number of graphite nodules, ΔT_L^g is undercooling according to graphite liquidus, f_L is fraction of remaining liquid and A_n and n are nucleation constants. It was found that $A_n = 4\times10^{11}$ $m^{-3}K^{-1}$ and n = 1 fits well with nodule count compared to the experiment.

An important factor for the growth of graphite nodules and austenite shell during solidification is the diffusion coefficient of carbon in austenite D_C^γ (m^2s^{-1}). Based on work by Ågren [9] and an average mol fraction of C in austenite of 0.073 the diffusion coefficient is found to be:

$$D_C^\gamma = 1.56\times10^{-5} \times \exp\left(\frac{-15260}{T}\right)$$

where temperature T is expressed in degrees Kelvin.

Examples of simulated cooling curves and corresponding dT/dt curves are shown in Fig. 2 – 5 together with measured cooling and dT/dt curves. The calculated temperature, nodule count and percent off-eutectic austenite are shown in Table 3.

4. Discussion

In the thin plates the first peak on the measured dT/dt curve (Fig. 2 and 3) can only be explained by nucleation and growth of austenite. If it was an arrest of primary graphite it should only be present in the hypereutectic plate and it should be present in the thicker plates, Fig. 4. However this is not the case.

The simulated dT/dt curves all have a peak corresponding to what is seen on the measured dT/dt curve in the thin plates. This peak arises from the start of growth of off-eutectic austenite when the solidification path reaches the austenite liquidus of the metastable extrapolation of it. In the model the undercooling for nucleation of austenite is neglected and therefore the peak on the simulated dT/dt curve is rather sharp compared to that on the measured dT/dt curve.

In the thicker plates (see Fig. 4 and 5) this first peak is not present on the measured dT/dt curve. This can be explained by that the nucleation of off-eutectic austenite and the arrest of the eutectic solidification contribute to the same peak of the measured dT/dt curve. This also explains the relatively large peak on the measured dT/dt curve, which is not present on the simulated dT/dt curve.

For the hypereutectic melt the presence of primary graphite nodules makes nucleation of austenite easy when the solidification path reaches the extrapolation of the austenite liquidus. This will not be the case in eutectic melt and higher undercooling will properly be required to nucleate austenite. For hypoeutectic alloys at relatively slow cooling rate (5-20°C/min) undercooling of 12-17°C have been reported for the nucleation of austenite [10]. This explains the higher undercooling in the eutectic melts compared to the hypereutectic ones. The large undercooling required for nucleation of the two phases, austenite and graphite, will also give a large driving force for the following growth of the phases. Therefore the eutectic melts will have a higher recalescence during solidification compared to the hypereutectic melts. The fact that nucleation of austenite is neglected in the numerical model has therefore a larger consequence for eutectic melts compared to hypereutectic ones because of different conditions for nucleation of austenite.

Regarding the amount of off-eutectic austenite, the numerical results shows that it will be present in both eutectic and hypereutectic melt. The eutectic melt will have more off-eutectic austenite compared to hypereutectic. Decreasing the plate thickness will increase the amount of off-eutectic austenite.

The calculated nodule count for the different plate thicknesses is very similar to nodule count in the experiments. The measured and simulated dT/dt curves fits well.

The simulated temperature is higher compared to the temperature measured in the experiments. However when measuring temperature with a thermocouple in castings, the presence of a thermocouple will affect the local solidification process, especially in thin wall castings. Simulation of temperature measurement in thin wall casting using a commercial 3-D simulation software shows that the shape of the measured temperature curve is correct but the measured temperature will be 15-20°C below the actual temperature in the plates during solidification [11]. In addition to that the simulated curves will be shifted down if some undercooling was allowed for nucleation of austenite.

5. Conclusion

The eutectic melts had larger undercooling and recalescence compared to the hypereutectic melts. The plate thicknesses from 2.8 to 8 mm had only a minor influence on the recalescence.

Austenite dendrites where present in the hypereutectic melts. The effect was more pronounced in thinner plates than in the thicker plates.

In the plates thinner than 4.3 mm, the solidification was divided into two stages. The first stage was small and can be explained by nucleation and growth of off-eutectic austenite or austenite dendrites. In the 8 mm plates the solidification had only one major stage.

The effect in thin plates of dividing the solidification into two stages was confirmed by the numerical simulation.

The simulated results show much smaller undercooling than the measured experimentally; however the cooling rates match well the experimental ones.

An improvement regarding nucleation of austenite needs to be done in order to improve simulations of especially the eutectic melts.

References

[1] D.K.Banerjee, D.M.Stefanescu, AFS Transactions 99 (1991) 747-759.
[2] T.Benecke, S.Venkateswaran, W.D.Schubert, B.Lux, The Foundryman 89 (1994) 355-360.
[3] C.F.Yeung, H.Zhao, W.B.Lee, Materials Characterization 40 (1998) 201-208.
[4] G.Rivera, J.Sikora, R.Boeri, AFS Transactions (2003) 979-990.
[5] G.Lesoult, M.Castro, J.Lacaze, Acta Materialia 46 (1998) 983-995.
[6] E.E.Underwood, Quantitative Stereology, Addison-Wesley Publishing Company, 1970.
[7] E.Weck, E.Leistner, Metallographic instructions for colour etching by immersion, Deutsher Verlag für Schweisstechnik (DVS) GmbH, Düsseldorf, 1982.
[8] J.Lacaze, M.Castro, G.Lesoult, Acta Materialia 46 (1998) 997-1010.
[9] J.Ågren, Scripta Metallurgica 20 (1986) 1507-1510.
[10] H.Miyake, A.Okada, AFS Transactions 106 (1998) 581-587.
[11] K. M. Pedersen and N. Tiedje. *Temperature measurement during solidification of thin wall ductile cast iron. Part 2: Numerical simulations.* Measurement. Measurement, in press, doi:10.1016/j.measurement.2007.05.003

Appendix

Details for the numerical modeling, see [5] and [8]. In this paper the selected physical properties were: Density: $\rho^l = 6800$ kg m^{-3} for liquid, $\rho^\gamma = 7000$ kg m^{-3} for austenite, $\rho^g = 2200$ kg m^{-3} for liquid and $\rho^m = 1550$ kg m^{-3} for mould. Specific heat capacity: $c_p^l = 920$ JK^{-1}kg^{-1} for liquid, $c_p^s = 750$ JK^{-1}kg^{-1} for solid and $c_p^m = 1200$ JK^{-}

$^{1}kg^{-1}$ for mould. The heat conductivity was set to 25 and 0.9 $WK^{-1}m^{-1}$ for the casting and mould respectively. The heat transfer coefficient HTC between casting and mould was constant 1000 $Wm^{-2}K^{-1}$. During primary disposition of graphite the diffusion of carbon in liquid, D_C^L, was set to 5.0×10^{-9} m^2s^{-1} and the constant K = 1 for the interfacial process between liquid and graphite. New nucleated graphite nodules were given an initial radius of $r_0^g = 0.5\times10^{-6}$m and the initial thickness of austenite shell around nodules during the eutectic stage was 1×10^{-6}m. The casting temperature was set to 1400°C in order to take into account the preheating of mould during filling.

Table 1 Chemical analysis and casting temperature (CE = %C + 0.28×%Si)

Casting	%C	%Si	%Mg	CE	Casting temperature [°C]
E	3.70	2.75	0.037	4.47	1340
F	3.51	2.70	0.030	4.27	1360
H	3.90	2.69	0.033	4.65	1370
J	3.57	2.64	0.028	4.31	1350

Table 2 Measured temperatures and nodule counts

Mould	Plate thickness [mm]	T_{12} [°C]	T_{min} [°C]	ΔT_{rec} [°C]	N [mm^{-3}]	Carbides
E1	8		1149.8	2.2	20740	
	4.3	1128.8	1125.3	1.7	29082	
	2.8	1111.1	1100.4	1.5	52229	
E2	8		1148.7	2.2	25861	
	4.3	1121.5	1120.2	1.0	34871	
	2.8	1121.8	1114.2	1.3	55585	
H1	8		-	-	37795	
	4.3	1109.4	1106.0	0.2	38333	
	2.8	1103.9	1091.4	3.2	68901	
H2	8		1131.3	2.5	30165	
	4.3	1107.7	1101.9	4.8	41377	<1%
	2.8	1098.4	1084.9	4.4	75694	
F3	8		1125.3	14.4	20859	
	4.3	1103.3	1099.2	17.9	32351	
	2.8	1094.1	1078.4	15.1	53910	~5%
J1	8		1113.7	15.1	15188	
	4.3		1091.1	21.5	32757	<1%
	2.8	1083.2	1081.4	20.5	54268	
J2	8		1114.7	14.8	14457	
	4.3		1090.6	21.5	32531	<1%
	2.8	1086.3	1082.0	20.0	65073	

Table 3 Results from numerical simulation (in case of no recalescence: T_{min} = Temperature at max dT/dt)

Casting	Plate thickness [mm]	T_{min} [°C]	ΔT_{rec} [°C]	N [mm^{-3}]	% off-eutectic austenite
E	8	1161.1	0.4	22875	5.8
	4.3	1152.7	1.5	39474	8.9
	2.8	1142.8	1.1	58904	13.1
H	8	1162.2	-	21722	5.7
	4.3	1154.3	-	37201	10.1
	2.8	1144.8	-	55296	14.9
F	8	1158.4	2.9	23534	11.4
	4.3	1149.7	3.4	39789	16.7
	2.8	1139.6	1.2	58136	23.1
J	8	1158.3	3.0	23889	8.9
	4.3	1149.7	3.6	40376	14.2
	2.8	1139.7	1.5	58833	20.6

Figures

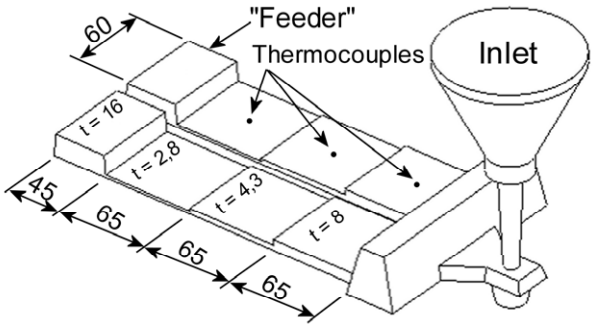

Fig. 1 Casting layout

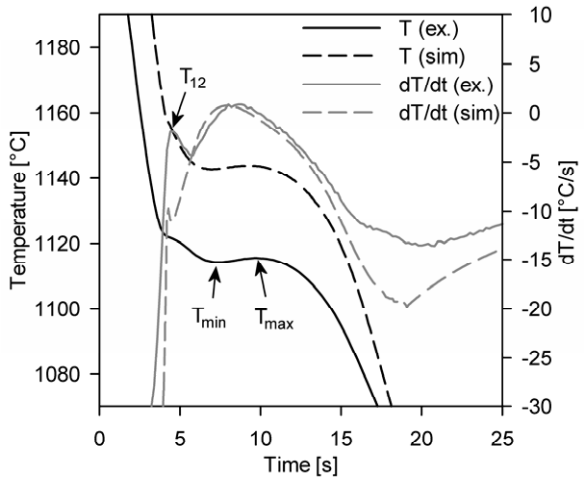

Fig. 2 Measured (casting E2, 2.8mm plate) and corresponding simulated cooling curve (full line experimental, dotted line simulated)

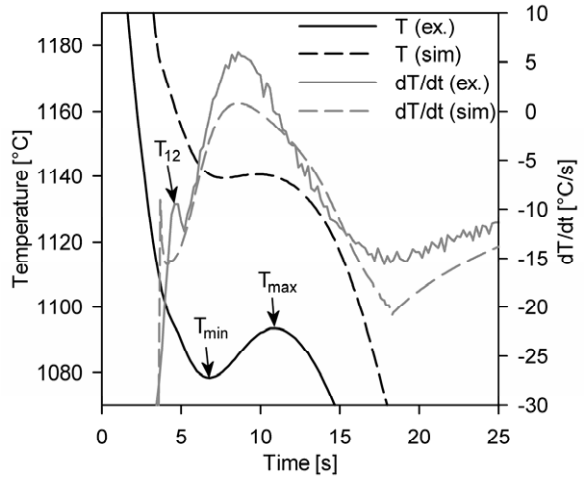

Fig. 3 Measured (casting F3, 2.8mm plate) and corresponding simulated cooling curve (full line experimental, dotted line simulated)

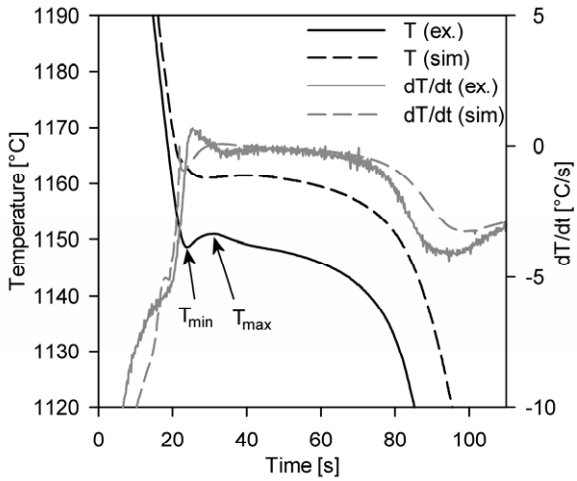

Fig. 4 Measured (casting E2, 8mm plate) and corresponding simulated cooling curve (full line experimental, dotted line simulated)

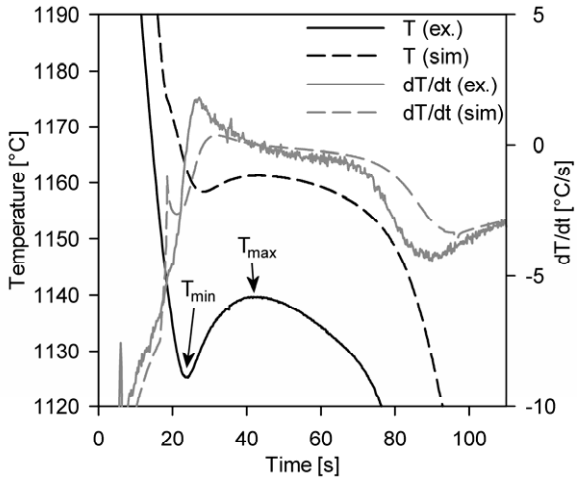

Fig. 5 Measured (casting F3, 8mm plate) and corresponding simulated cooling curves (full line experimental, dotted line simulated)

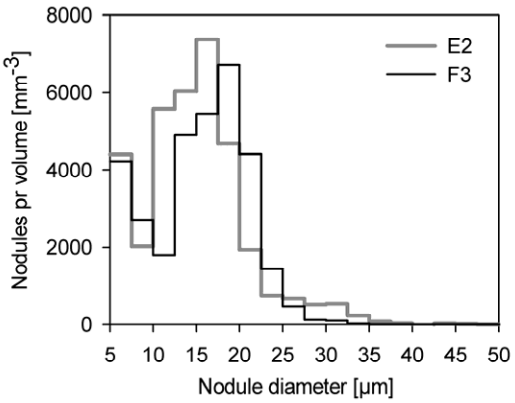

Fig. 6 Size distribution of nodules, casting E2 and F3; 4,3mm plate